Transport properties of random arrays of dielectric cylinders

A. Kirchner
Institut für Theorie der Kondensierten Materie, Universität Karlsruhe, 76128, Karlsruhe, Germany

K. Busch*
Institut für Theorie der Kondensierten Materie, Universität Karlsruhe, 76128, Karlsruhe, Germany
and Ames Laboratory and Department of Physics and Astronomy, Iowa State University, Ames, Iowa 50011

C. M. Soukoulis
Ames Laboratory and Department of Physics and Astronomy, Iowa State University, Ames, Iowa 50011
(Received 25 July 1997)

We apply a recently developed approach for calculating the transport properties of random media to the case of disordered arrays of parallel oriented and normally illuminated cylinders. Within this effective-medium theory resonant scattering of the individual scatterer is treated exactly, and by using a coated cylinder as the basic scattering unit, multiple scattering contributions are incorporated in a mean-field sense. In the long-wavelength limit we are able to calculate the effective dielectric constant analytically. We compare our findings with results for periodic systems. For both ''scalar'' and ''vector'' polarization, we reliably calculate the mean-free path, the transport velocity, and the diffusion coefficient for finite frequencies for all densities of scatterers and dielectric contrasts. Furthermore, within this effective-medium approach, we present our results for the localization parameter $\overline{k\ell}_t$ for both two- and three-dimensional systems, thereby identifying the optimal parameters for observing localization. [S0163-1829(97)02546-0]

I. INTRODUCTION

The interest in studying the propagation of classical waves in strongly scattering random media has experienced a considerable boost over the last decade.[1,2] Starting with the observation of the coherent backscattering effect in classical wave systems,[3] the analogous effect to weak localization in the electronic case, it has soon been realized that many quantum effects have their analogy in classical wave systems. This has opened the field for technological applications like photonic band-gap materials[4] as well as new fundamental research such as the photonic Hall effect[5] and anisotropic light diffusion.[6].

Although the analogy between quantum and classical waves carries very far, there are certain differences that do not allow a simple translation of the many results of disordered electronic to strongly scattering classical wave systems: For example, the Anderson localization[7] of classical waves has not been observed as yet, despite the fact that theoretical work[8] indicated its existence in an intermediate frequency regime and recent experimental investigations[9,10] along these lines reported very low values for the diffusion coefficient D. In fact, the pioneering work of van Albada *et al.*[9] showed that, unlike electronic systems, there exists another renormalization mechanism of the diffusion coefficient D for classical waves. Using a scalar theory in the low density regime, van Albada *et al.*[9] were able to show that the presence of resonant scatterers may cause the energy transport velocity v_E to decrease sharply close to the single-scatterer resonances. This renormalized transport velocity enters the three-dimensional diffusion coefficient via $D=v_E\ell_t/3$,[10,11] where ℓ_t is the transport mean free path. It can be viewed as either being the result of a different Ward-Identity due to an energy-dependent scattering potential (microscopic viewpoint) or caused by a scattering delay due to temporal storage of wave energy inside the scatterers (phenomenological viewpoint). In addition, yet another renormalization mechanism, which originates in the asymmetric scattering from finite sized spheres, has recently been identified by Livdan and Lisyansky.[12] In contrast to the above-mentioned energy-storage effect this asymmetry renormalizes the transport mean free path ℓ_t rather than the energy transport velocity v_E. In the low-density regime it smoothens the very sharp spikes of the ripple structure, which is superimposed on the much broader Mie resonance structure of the energy transport velocity renormalization. However, while these additional corrections are certainly very important for quantitative considerations they do not change the overall physical picture. In essence, considerable care has to be exerted when interpreting low values of the diffusion coefficient D for classical wave systems.

Besides the presence of Mie resonances in the intermediate frequency regime, polarization effects may play an additionally important role for electromagnetic (EM) waves. The different polarizations of the EM waves have to be taken into account on a full vector calculation in deriving the Boltzmann equation, starting from the Bethe-Salpeter equation, a task that has been partially solved only very recently.[13] In addition, experimental results[10] for alumina spheres have shown that as the volume fraction of the scatterers f increases towards close packing ($f\simeq 0.60$), there is no structure in the diffusion coefficient versus frequency. This clearly suggests that there is no structure in the transport velocity. Such a behavior is not observed when extending the low-density theory of van Albada *et al.*[9] to this high f regime. Thus, it is by now well understood that to *lowest order in*

density of the dielectric scatterers, the strong decrease in the transport velocity is due to the (single scatterer) Mie resonances. For higher values of the density multiple-scattering corrections become appreciable and tend to wash out the single-scatterer resonances, as observed experimentally.[10] In the spirit of the coherent-potential approximation (CPA) a conceptually different approach to the problem of classical wave propagation in strongly scattering random media has recently been developed[14] and obtained CPA velocities for high densities of scatterers, which has been qualitatively consistent with experiment, in not showing any structure as a function of frequency. Not surprisingly, the newly developed[14] coated CPA for low f gives a CPA velocity that reduces to the regular phase velocity that may exceed the velocity of light near Mie resonances. This is an undesirable feature of the CPA that can be understood to be the result of underestimating the above-mentioned energy-storage effect. Thus, for small f, it is the theory of van Albada *et al.*[9] that seems to give the correct energy transport velocity v_E, while for large f, it is the coated CPA approach[14] that appears to give energy transport velocities consistent with experiment.[10]

In an effort to investigate the differences between scalar classical waves and the vector character of EM waves, both theories, the low-density theory of van Albada *et al.* and the coated CPA, have recently been extended to the two-dimensional case, i.e., to random arrangements of parallel oriented and normally illuminated cylinders.[15] In such systems, the two polarizations of an EM wave decouple, effectively leading to two separate problems: If the light is polarized parallel to the cylinders axis a standard scalar wave problem is obtained, whereas the polarization perpendicular to the cylinders axis manifests the vector character of the EM waves in, e.g., the absence of s-wave scattering. Pronounced differences between these two polarizations have already been reported for ordered systems, i.e., the band structure of two-dimensional photonic crystals differ substantially for scalar and vector polarization.[16] Similarly, the application of the low-density theory of van Albada *et al.*[15] as well as the coated CPA (Ref. 15) revealed pronounced differences in their respective regimes of applicabilty. However, the coated CPA has been somewhat hampered by numerical problems and not very reliable statements, especially concerning localization, could be made. Recent numerical studies,[17] however, clearly demonstrate that localization for high dielectric cylinders in a low dielectric medium is achieved much more easily for the scalar-polarized than it is for the vector-polarized case.

The above situation with different theories for different parameter regimes and the lack of an interpolation scheme between them is clearly very unsatisfactory. Therefore, two of us have recently developed an approach to the problem of classical wave propagation in random media.[18,19] This effective-medium theory captures the effects of resonant scattering from single scatterers exactly and incorporates multiple-scattering effects in a mean-field sense. Its application to three-dimensional systems has led to results for all transport quantities consistent with the theory of van Albada *et al.*[9] in the low-density regime as well as with the coated CPA (Ref. 14) in the high-density regime. In addition, without adjustable parameters, the effective-medium theory has obtained quantitative agreement with experiments in the strong scattering regime.[19] In view of the above discussion, attempting to apply the new effective-medium theory to two-dimensional systems appears to be very desirable, indeed. In the present paper, we, therefore, report the findings of our investigation of the transport properties of classical waves in two-dimensional random media within the framework of this effective-medium theory.

The paper is organized as follows. In Sec. II we review the formalism of the new effective-medium theory and apply it to two-dimensonal systems. For the long-wavelength limit, analytical results are presented in Sec. III. In addition, we contrast these findings with results for the effective dielectric constant of two-dimensional photonic crystals. Section IV contains detailed results on transport properties for finite frequencies such as the mean free path, energy transport velocity, and diffusion coefficient for various densities of scatterers and dielectric contrasts. In Sec. V we present results on the localization parameter $\overline{k\ell}_t$ obtained within this approach. The optimal parameters and structures for achieving localization are discussed. Finally, Sec. VI is devoted to a discussion of the results and in the Appendixes we clarify some notational matters for scattering of EM waves by cylinders and give details of calculations that would unnecessarily complicate the text.

II. THE EFFECTIVE-MEDIUM THEORY

We consider a composite medium of two lossless materials, with dielectric constants ϵ_1 and ϵ_2. Our composite medium is assumed to consist of infinitely extended, parallel oriented, and randomly placed cylinders with diameter $d=2R$ and dielectric constant ϵ_1 embedded within a host material with dielectric constant ϵ_2. The random medium is characterized also by f, the volume fraction occupied by the cylinders.

The basic idea of any effective-medium theory of disordered systems is to focus on one particular scatterer and to replace the surrounding random medium by an effective homogeneous medium. The effective medium is determined self-consistently by taking into account the fact that any other scatterer could have been chosen. This procedure manifests the homogeneity of the random medium on average. In conventional effective-medium theories, such as the CPA, the effective medium is determined by demanding that the total cross section (TCS) of the difference between scattering medium and the effective medium vanishes on average[14,15,20] or takes on a minimal value.[21,22] In the effective medium the energy density is homogeneous by construction.

However, the position of a cylinder in the medium is completely random, with the exception that the cylinders cannot overlap. This implies that the distribution $P(R)$ of spacings between neighboring cylinders is sharply peaked at a distance $R_c > R$. If we approximate this distribution by a δ function, i.e., $P(R) \propto \delta(R_c - R)$ and take into account the on-average isotropy of the random medium, we may consider a coated cylinder as the basic scattering unit. The radius R_c of the coated cylinder is $R_c = R/f^{1/2}$. The dielectric constants of the core and the coating are ϵ_1 and ϵ_2, respectively. Using a coated cylinder as the basic scattering unit also incorporates some of the multiple-scattering effects at different centers.

With this technique it is, therefore, possible to obtain reliable information about transport properties for the whole range of disorder, i.e., all values of scatterer density and dielectric contrast, as has been demonstrated in recent works.[18,19,21,22]

The use of a coated cylinder as the basic scattering unit also implies that the homogeneity of the energy density is not anymore trivially fulfilled. This is where the conventional CPA for electrons fails for classical waves: In the intermediate frequency or Mie scattering regime of classical wave systems the internal (shape) resonances of the scatterers may be thought of as resonant cavities that lead to a temporary energy storage inside the scatterers, i.e., to a scattering delay that the conventional CPA does not fully account for in the low-density regime where the coating radius R_c is large. Therefore, in the new effective-medium theory[18,19] we explicitly chose the averaged energy density homogeneity as the criterion for determining the effective medium. Since we are exclusively considering lossless dielectrics the effective-medium dielectric constant $\overline{\epsilon}$ has to be real due to energy conservation. This is in contrast to the conventional approaches and forces us to proceed in two steps: First, we determine for every frequency ω the real effective dielectric constant $\overline{\epsilon}$ by demanding the *energy density to be homogeneous on scales larger than the basic scattering unit* (coated cylinder). Then, in a second step, the physical quantities are calculated from the (now nonvanishing) scattering cross sections. In this theory all multiple scattering effects are contained in the effective dielectric constant and, thus, we may consider the random medium as consisting of independent scatterering units, i.e., coated cylinders, immersed in the effective medium.

Since in the above-mentioned arrangement the effective-medium dielectric constant is real and the energy density is homogeneous on scales larger than the basic scattering unit, we may neglect the energy-storage effect in calculating the energy transport velocity v_E. Accordingly, v_E may now be obtained from the phase velocity v_p, i.e., $v_E = c_m^2/v_p$,[19,22] where $c_m = c/\sqrt{\overline{\epsilon}}$. v_p, in turn, is determined by the TCS (or equivalently by the self-energy Σ) of a coated cylinder embedded in the effective medium: $v_p = c_m/\sqrt{1 - \mathrm{Re}(\Sigma)/k_m^2}$, where $k_m = \omega/c_m$. The requirement that the energy content per unit length of a coated cylinder embedded in the effective medium and being hit by a plane wave should be the same as the energy stored by the plane wave in an equally sized volume of the effective medium can be formulated quantitatively by the self-consistency equation

$$\int_0^{R_c} d^2 r \rho_E^{(1)}(\vec{r}) = \int_0^{R_c} d^2 r \rho_E^{(2)}(\vec{r}), \tag{1}$$

where $\vec{r}$ is a two-dimensional vector. $\rho_E^{(1)}(\vec{r})$ and $\rho_E^{(2)}(\vec{r})$ are the energy densities per unit length for a coated cylinder and a plane wave, respectively. Clearly, this very general principle can be applied to any kind of classical wave propagation, such as, e.g., elastic waves.[23]

In the present case, the energy density of EM waves with electric and magnetic fields, $\vec{E}(\vec{r})$ and $\vec{H}(\vec{r})$, is given by

$$\rho_E(\vec{r}) = \frac{1}{2}[\epsilon(\vec{r})|\vec{E}(\vec{r})|^2 + \mu|\vec{H}(\vec{r})|^2]. \tag{2}$$

Here, μ is the magnetic permeability, which is taken to be the same in both materials. The specific form of the scattered fields inside the coating and the core are given in Appendix A, Eqs. (A3) and (A4) and the complete evaluation of the integral on the left-hand side of Eq. (1) is described in Appendix B, Eqs. (B2) and (B3). At this point it suffices to note that while the right-hand side of Eq. (1) is an obvious function of the effective-medium dielectric constant $\overline{\epsilon}$, the left-hand side through its complicated dependence of the fields' scattering coefficients [c.f. Eqs. (B2) and (B3) as well as Eqs. (A9)–(A30)] is a nontrivial function of the effective-medium dielectric constant $\overline{\epsilon}$, too. Consequently, Eq. (1) together with Eq. (2) and the respective expressions for the fields determine the (real) dielectric constant $\overline{\epsilon}$ of the effective medium for every frequency. The differences between the two polarizations enter via the different scattered wave fields needed for evaluating the left-hand side of Eq. (1). As mentioned above, the energy transport velocity v_E is obtained from the phase velcity $\overline{v_p}$ (Refs. 19 and 22) and the renormalized wave vector $\overline{k}$ as well as the scattering mean free path ℓ_s can be calculated via[19,22]

$$v_E \simeq \frac{c}{\sqrt{\overline{\epsilon}}}\sqrt{1 - \mathrm{Re}(\Sigma)/k_m^2}, \tag{3}$$

$$\ell_s = \frac{1}{\sqrt{2}\,\mathrm{Im}(\Sigma)}\{[k_m^2 - \mathrm{Re}(\Sigma)] + \sqrt{[k_m^2 - \mathrm{Re}(\Sigma)]^2 + [\mathrm{Im}(\Sigma)]^2}\}^{1/2}, \tag{4}$$

$$\overline{k} = \frac{1}{\sqrt{2}}\{[k_m^2 - \mathrm{Re}(\Sigma)] + \sqrt{[k_m^2 - \mathrm{Re}(\Sigma)]^2 + [\mathrm{Im}(\Sigma)]^2}\}^{1/2}. \tag{5}$$

All the multiple scattering contributions enter the new effective-theory through the effective dielectric constant $\overline{\epsilon}$, which allows us to calculate the self-energy Σ in the independent scatterer approximation:

$$\Sigma = n t_{\vec{k}\vec{k}}(\omega), \tag{6}$$

where, $t_{\vec{k}\vec{k}'}(\omega)$ denotes the t matrix of a coated cylinder embedded in the effective medium, $|\vec{k}|$ is equal to k_m, and $n = 1/R_c^2$ is the density of scatterers. We have that

$$t_{\vec{k}\vec{k}}(\omega) = -4i\left(a_0^{\parallel/\perp} + 2\sum_{l=0}^{\infty} a_l^{\parallel/\perp}\right). \tag{7}$$

Here $a_l^{\parallel/\perp}$ denote the scattering coefficients for the outside field, i.e., $a_l^{\parallel} = D_l^{\parallel}$ and $a_l^{\perp} = -iC_l^{\perp}$ (c.f. Appendix A). Furthermore, in the same spirit as that in which we obtained the energy transport velocity, we approximate the transport mean free path ℓ_t by the scattering mean free path ℓ_s, i.e., $\ell_t \approx \ell_s$. Then, the two-dimensional diffusion constant D is given by $D = v_E \ell_t/2$. This approximation is supported by the fact that, as a mean-field theory, the new effective-medium theory is unable to make detailed predictions close to the Anderson transition where the distinction between scattering and transport mean free paths would become important. In

addition, previous studies of the transport and scattering mean free paths[14] obtained results consistent with this approximation.

The above set of formulas comprises the basis of the new effective-medium theory. In what follows we first examine their long-wavelength limit, where analytical results can be derived. For finite frequencies numerical studies have to be performed.

III. LONG-WAVELENGTH LIMIT

If a wave with wavelength much larger than the scatterer size and mean scatterer spacing propagates through a random medium, it cannot resolve the disorder and, therefore, we may define a frequency-independent, long-wavelength dielectric constant ϵ_∞ according to

$$\epsilon_\infty = \lim_{\omega\to 0}\left(\frac{c}{v_{\mathrm{E}}(\omega)}\right)^2. \tag{8}$$

The theory of such long-wavelength dielectric constants for EM waves itself is an old but, nevertheless, still very active field. Without trying to be complete, we want to mention the classic theories of Brüggeman[24] and Maxwell-Garnett[25] and the more modern works of Bergman,[26] who showed that the classic theories follow from a more general expression by making special choices for the so-called Bergman spectral function.

The main difference between three-dimensional Maxwell-Garnett and Brüggeman theory lies in the topology of the random medium. While Maxwell-Garnett theory considers isolated spheres of one dielectric constant embedded in a material with different dielectric constant, Brüggeman theory starts from a symmetric arrangement of ''lumps'' of both materials. As a consequence, Brüggeman theory leads to an expression for the long-wavelength dielectric constant that is symmetric upon interchanging the two dielectric constants ϵ_1 and ϵ_2 as well as f with $1-f$, where f is the filling fraction of one type of material. In contrast, Maxwell-Garnett theory leads to a formula that does not exhibit this symmetry. For the topology of our model system, i.e., cylinders of dielectric constant ϵ_1 embedded in a medium with dielectric constant ϵ_2 and a filling fraction f of the cylinders, it is well known[22] that the scalar case is insensitive to this distinction and the correct result for ϵ_∞ is given by the volume averaged dielectric constant, whereas in the vector case it is Maxwell-Garnett theory which gives the right answer. To calculate ϵ_∞ within the new effective medium theory, according to Eq. (8), we, first, need to compute $\overline{\epsilon}$ for $\omega\to 0$ from Eq. (1) using a Taylor expansions of all quantities involved to extract the leading order in ω. Then we use this results to obtain an expression for $v_{\mathrm{E}}(\omega)$ as $\omega\to 0$ from Eq. (8) in connection with Eqs. (3) and (6).

The calculations are very straightforward but also very tedious and proceed along the same lines as outlined in Ref. 19, so that we may only state the results. Indeed, in the case of scalar polarization we obtain as the long-wavelength dielectric constant the volume avarage of ϵ_1 and ϵ_2, i.e.,

$$\epsilon_\infty^{\parallel} \equiv \overline{\epsilon} \equiv f\epsilon_1 + (1-f)\epsilon_2. \tag{9}$$

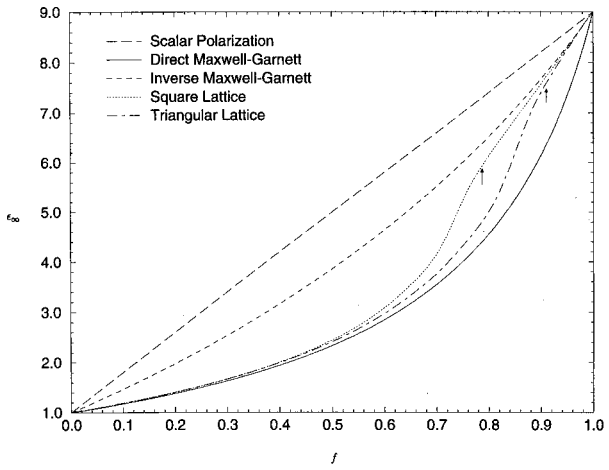

FIG. 1. Long-wavelength dielectric constants for various structures as a function of the filling fraction f for dielectric constants $\epsilon_1=9$ (cylinders) and $\epsilon_2=1$. Arrows indicate the filling factors f_0 for which the cylinders of the two-dimensional photonic crystals start overlapping.

This result originates from the fact that for the scalar polarization s-wave scattering dominates in the long wavelength limit.

In the case of the vector polarization, however, s-wave scattering is absent and a careful analysis of the dominant p-wave scattering for long wavelengths in Eq. (8) leads indeed to the expected Maxwell-Garnett result, i.e.,

$$\epsilon_\infty^{\perp} = \overline{\epsilon} = \epsilon_2\left(1+\frac{2f\alpha}{1-f\alpha}\right), \tag{10}$$

where $\alpha=(\epsilon_1-\epsilon_2)/(\epsilon_1+\epsilon_2)$ is the depolarization factor of the cylinder for the vector polarization. In order to obtain more insight into Eqs. (9) and (10) we wish to compare them to the long-wavelength limit of corresponding ordered systems, i.e., with long-wavelength dielectric constants obtained from the linear part of the dispersion relation of photonic band structures with respective filling factors f. Since in the long-wavelength limit the wave can neither resolve the disorder of the random medium nor the structure of the photonic crystal, we expect the results of this study to be similar if not identical to the results of the new effective-medium theory for respective polarizations. However, in the photonic crystal, we may state exactly for which filling ratio the cylinders start to overlap, effectively changing the topology of the system. This is a feature that is absent in the effective-medium theory for obvious reasons.

For periodic structures, the most straightforward approach is to operate in Fourier space, where the periodic boundary condition can be put in trivially by imposing Bloch's theorem.[27] We leave details of the calculation for Appendix C and report here only the results: For the scalar polarization we, once again, obtain the volume average of the two dielectric constants, i.e., Eq. (9) as the long-wavelength dielectric constant for a two-dimensional photonic crystal. In Fig. 1 we show results for the long-wavelength dielectric constant for the vector polarized case for a square (dotted line) and a triangular lattice (dashed-dotted line). The arrows indicate at which filling fraction the high dielectric cylinders start to

overlap. In addition, we plotted in Fig. 1 the two versions of the Maxwell-Garnett theory that are obtained from interchanging the dielectric constants and the filling fractions f and $1-f$. In what follows we will refer to these two structures as the direct (solid line) and the inverse structure (dashed line), respectively, where we assume, without loss of generality, that $\epsilon_1 > \epsilon_2$. Here we have in mind that the direct structure usually consists of free standing high dielectric cylinders in air,[16] whereas the inverse structure is most commonly manufactured by drilling cylindrical holes in a block of high dielectric material.[16]

Obviously, the long wavelength dielectric constants of photonic crystals for the vector polarization are reasonably well described by the Maxwell-Garnett result for small and very high f. However, around the filling factor f_0 for which the cylinders start to overlap, we observe a crossover from direct to inverse Maxwell-Garnett theory. This clearly confirms the above-mentioned importance of topology. Similar results, albeit using a different technique, have been obtained previously.[28] At this point, we want to mention that the importance of topology will play a role for the localization of classical waves, too (c.f. Sec. V).

IV. FINITE FREQUENCIES

For finite frequencies, of course, no analytical solution of Eq. (1) is possible. Fortunately, it turns out that Eq. (1) is numerically much easier to deal with than the self-consistency equations of the coated CPA approach.[14,15] To obtain a converged result, we used a simple fixpoint iteration with the long-wavelength limit as a starting value for the effective medium dielectric constant $\overline{\epsilon}$. The convergence (relative change of $\overline{\epsilon}$ from one iteration step to the next being less than 10^{-4}) was obtained in almost all cases with less than 10 iterations. After a successful convergence for $\overline{\epsilon}$ we compute the self-energy Σ according to Eq. (6) and then evalute Eq. (3) and Eq. (4) for the energy transport velocity v_E and the scattering mean free path ℓ_s, respectively. We chose to present these results for v_E and ℓ_s as a function of d/λ_i, where d is the diameter of the dielectric cylinders and $\lambda_i = 2\pi c/\omega\sqrt{\epsilon_1}$ is the wavelength inside the cylinders. The reason behind that is the fact that strong Mie resonances of the isolated cylinder appear in the limit $\epsilon_1/\epsilon_2 \to \infty$ at $d/\lambda_i = (n+1)/2$, with $n = 1,2,3\ldots$ for the vector and $n = 0,1,2,\ldots$ for the scalar case. Furthermore, it should be noted that we used different numbers of scattering coefficients in the series given by the left-hand side of Eq. (1), i.e., in Eqs. (B2) and (B3). We found that increasing the maximal number of scattering coefficients beyond 25 does not alter the results in the range of d/λ_i that we have considered.

Figures 2(a) and 2(b) show the scattering mean free path ℓ_s in units of the cylinder radius R for scalar and vector classical waves, respectively, versus d/λ_i for a possible future experimental setup similar to the one used for demonstrating the existence of photonic band gaps.[16] This setup consisted of long (as compared to their diameter) alumina cylinders ($\epsilon_1 = 9$) standing freely ($\epsilon_2 \approx 1$) in an anechoic chamber, for which different values of the filling factor f of the alumina cylinders can easily be realized. Figures showing the energy transport velocity v_E for scalar and vector classical waves, respectively, versus d/λ_i for the same configurations are shown in Figs. 3(a) and 3(b). A direct measurement of the energy transport velocity as a function of frequency along the lines of Ref. 29 rather than an indirect measurement via diffusion coefficient and transport mean free path could validate the interesting behavior predicted in these figures. In particular, the absence of s-wave scattering for the vector polarization leads to pronounced differences around the first Mie resonance.

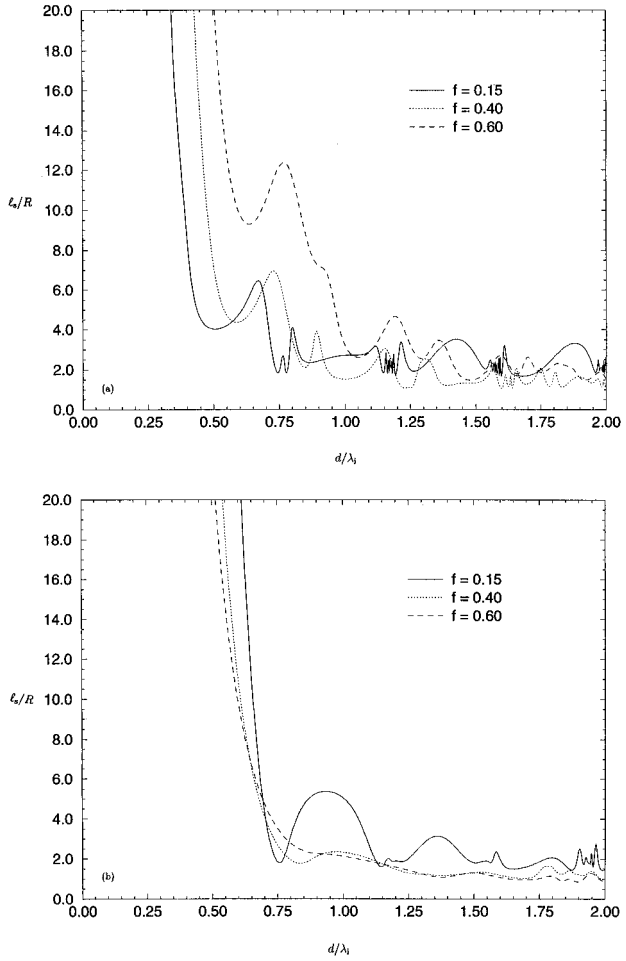

FIG. 2. The scattering mean free path ℓ_s for the scalar (a) and vector (b) polarization in units of the cylinder radius R as a function of d/λ_i for filling fractions $f = 0.15$ (solid line), $f = 0.4$ (dotted line), and $f = 0.6$ (dashed line), respectively. The values of the dielectric constants are $\epsilon_1 = 9$ (cylinders) and $\epsilon_2 = 1$.

It can be seen that for low values of the filling factor v_E exhibits large dips near the Mie resonances that become smeared out as the filling factor increases. This behavior is in conformity with the fact that due to the multiple-scattering contributions the effective medium gets stronger renormalized as f increases, thus competing with the single scatterer effects which dominate at low filling factors f. Clearly a low-density theory is unable to capture this effect (for figures of v_E vs d/λ_i for similar parameter values, we refer to Ref. 15). However, the qualitative behavior of v_E (or rather D) as a function of frequency for various filling fractions f has been confirmed by experiment[10] only for the three-dimensional case.

We also investigated the behavior of the inverse structure,

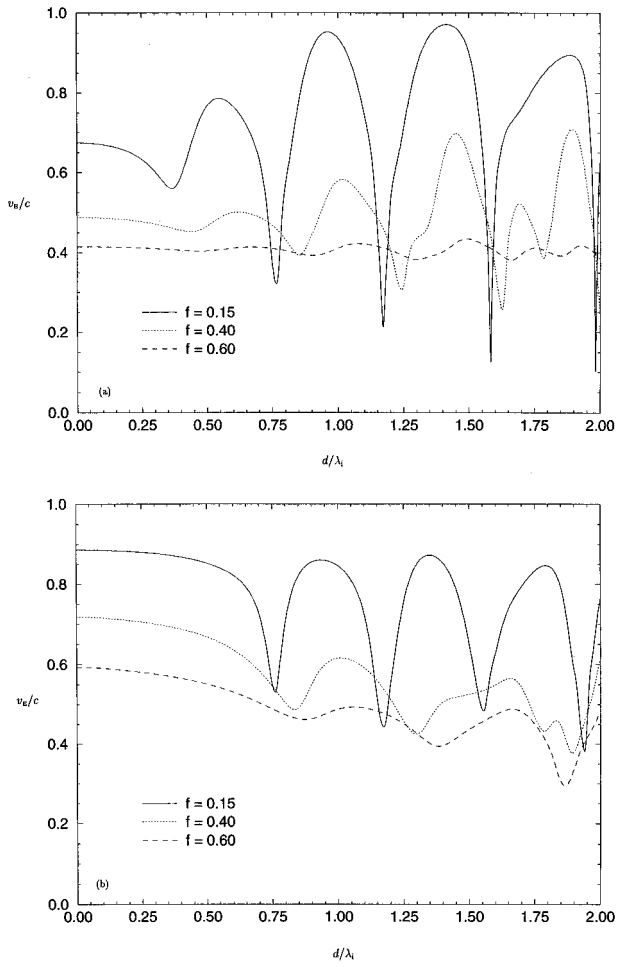

FIG. 3. The energy transport velocity v_E for the scalar (a) and vector (b) polarization in units of the vacuum speed of light c as a function of d/λ_i for filling fractions $f=0.15$ (solid line), $f=0.4$ (dotted line), and $f=0.6$ (dashed line), respectively. The values of the dielectric constants are $\epsilon_1=9$ (cylinders) and $\epsilon_2=1$.

i.e., cylinders of low dielectric material situated in a high dielectric material matrix. Such systems, like air cylinders etched into macroporous silicon, have recently been investigated experimentally in the context of photonic crystals[16] and, as will be discussed in the following section, may provide a better environment for observing the localizaton of classical waves in both two and three dimensions. For the inverse structure, the numerical effort to obtain converged results increases drastically for parameter regimes in which the localization parameter $\overline{k}\ell_t$ takes on very low values (c.f. Sec. V). We attribute this fact to the upcoming of a breakdown of the effective-medium theory for strongly localized waves: Near the Anderson transition or inside the localized regime a mean-field theory does not anymore adequately describe the system. However, in terms of the behavior of the scattering mean free path ℓ_s or the energy transport velocity v_E we did not find a qualitative difference to the direct structure (high dielectric material in low dielectric matrix).

V. STUDY OF THE LOCALIZATION PARAMETER

The product $\overline{k}\ell_t$, where $\overline{k}$ is the renormalized wave vector and ℓ_t the transport mean free path, is a measure for the strength of the multiple-scattering effects. Here, we wish to recall that within the effective-medium theory we have $\ell_t \approx \ell_s$. For $\overline{k}\ell_t \gg 1$ radiative transfer theory, which may be viewed as a Boltzmann theory for EM waves, becomes a good approximation. For values of $\overline{k}\ell_t \simeq 1$ this ceases to be a good description of the propagation of waves, since, speaking in the picture of Feynman paths, constructive interference of time-reversed paths notably renormalizes the diffusion coefficient and may ultimately lead to a change in wave functions' nature from extended to localized. This phenomenon, called Anderson localization,[7] is a generic wave property and may be studied in the context of classical waves, although is was originally proposed for electron waves. In fact, it is still an open problem whether classical waves can be localized in the sense of Anderson. There exist various theories that provide localization criteria for waves: if the value of $\overline{k}\ell_t$ falls below a certain value, localization is achieved. Probably, one of the most accurate among these is the potential well analogy,[30] which sets the critical value for $\overline{k}\ell_t$ to 0.844.

Clearly, in a mean-field theory like the new effective-medium theory no quantitative statements as to when a wave system is crossing from extended to localized can be made. However, the value of the localization parameter $\overline{k}\ell_t$ can still be evaluated and, as a function of the system parameters, may exhibit certain trends towards parameter values optimal for localization. In this spirit, we have performed a systematic study of the localization parameter $\overline{k}\ell_t$ as a function of the dielectric contrast ϵ_1/ϵ_2 and filling fraction f for scalar and vector polarization for the direct as well as for the inverse structure. We assigned to every parameter value combination the minimum of $\overline{k}\ell_t$ as a function of frequency. In this way we were able to obtain contours of constant $\overline{k}\ell_t$ value as a function of dielectric contrast and filling fraction. The results of this cumbersome study are displayed in Figs. 4(a) and 4(b) for scalar and vector polarization in the direct structure and in Figs. 5(a) and 5(b) for scalar and vector waves in the inverse structure. It is clearly seen that in all cases, for a given dielectric contrast there exists an optimal range of the filling fraction for which the localiation parameter $\overline{k}\ell_t$ takes on its lowest values. As the contrast increases, these ranges decrease, pointing towards an optimal filling ratio. For the direct structure the optimal filling ratio for both polarizations is around $f \approx 0.25$, whereas for the inverse structure, the scalar polarization has its optimal filling ratio at $f \approx 0.8$ while the vector polarization has its optimum around $f \approx 0.6$. Furthermore, the values for $\overline{k}\ell_t$ achieved within the same parameter range are much lower for the inverse structure than they are for the direct structure. As mentioned before, we conclude from this analysis that the inverse structure may be prefered when looking for localization of classical waves. Finally, in the direct structure, vector waves are much harder to localize than scalar waves as can be seen from comparing the values of $\overline{k}\ell_t$ of Fig. 4(a) with 4(b). This result has already been obtained on the basis of numerical simulations.[17] For the inverse structure, however, the opposite is true, i.e., vector waves are easier to localize than scalar waves. [c.f. Figs. 5(a) and 5(b)].

The interpretation of these results is transparent: In two

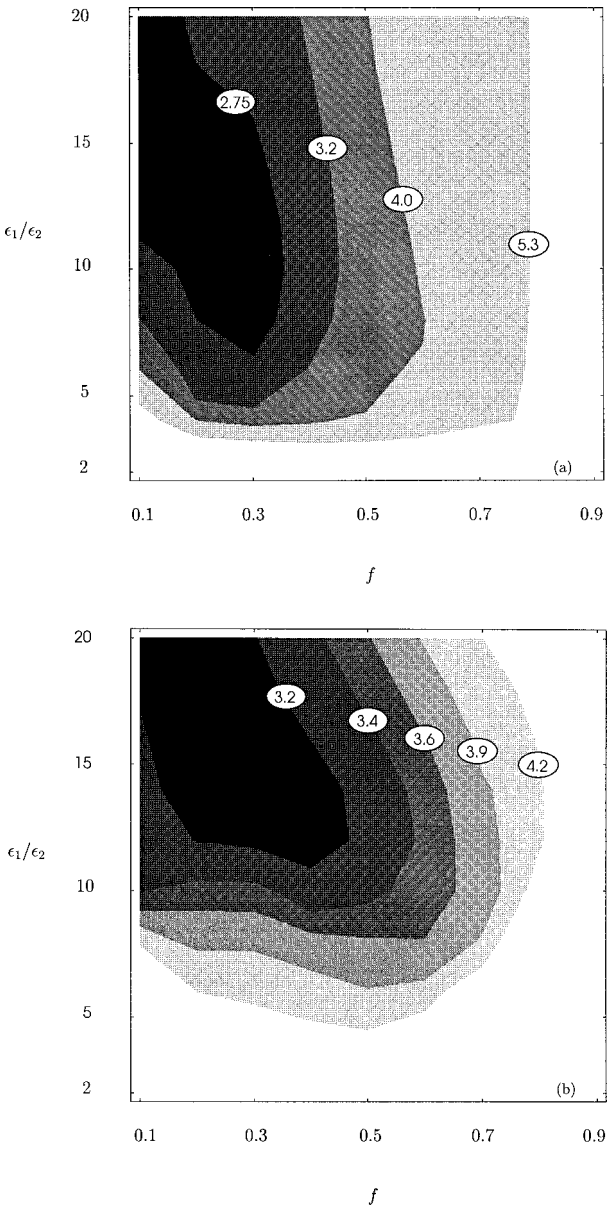

FIG. 4. Contour plot of the localization parameter $\overline{k\ell}_t$ for the scalar (a) and vector (b) polarization in the direct structure for various filling factors f and dielectric contrasts $\epsilon_1 > \epsilon_2$.

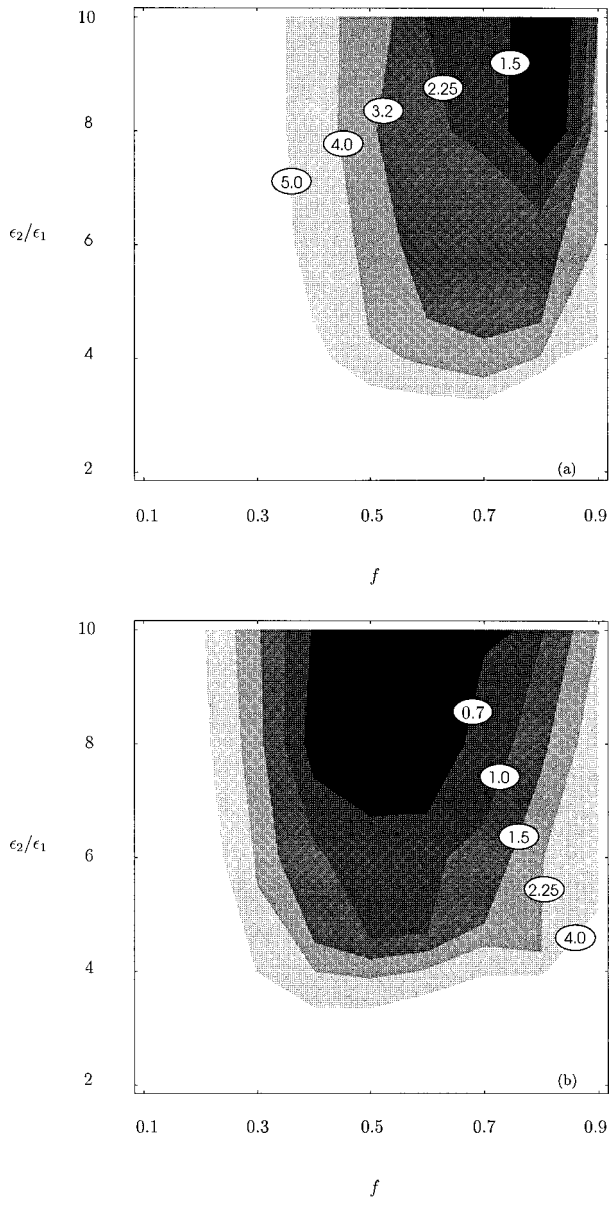

FIG. 5. Contour plot of the localization parameter $\overline{k\ell}_t$ for the scalar (a) and vector (b) polarization in the inverse structure for various filling factors f and dielectric contrasts $\epsilon_2 > \epsilon_1$.

dimensions we expect on the basis of the scaling theory of localization,[31] the waves to be always localized. However, the localization lengths may be very much different for different dielectric contrast ϵ_1/ϵ_2 and/or filling ratio f. Therefore, the above analysis of the localization parameter $\overline{k\ell}_t$ indicates the optimal parameter regime for realizing the smallest localization lengths. It would, therefore, be extremely interesting to measure the localization length for various scenarios, in order to compare with the above predictions. This could probably best be done along the lines or Ref. 32 in which similar experimental studies were carried out on one-dimensional systems. In addition, we have performed an analogous study of the localization parameter for EM waves in three dimensions. The results for the direct and the inverse structure are shown in Figs. 6(a) and 6(b), respectively. Here, too, we obtain that localization may be more easily achieved for the inverse structure, where the optimal filling factor f is around $f \approx 0.45$ for the direct and $f \approx 0.7$ for the inverse structure. However, the values for $\overline{k\ell}_t$ are generally much higher than in the corresponding parameter regime in two dimensions (the lowest values are around $\overline{k\ell}_t \approx 2.5$ for the contrast ranges considered above). This is certainly consistent with the results of the scaling theory of localization, which predicts that, in contrast to two-dimensional systems, there is a critical disorder to be exceeded in three dimensions before a wave becomes localized.

VI. DISCUSSION

In summary, we have succesfully applied the effective medium theory of Refs. 18 and 19 to two-dimensional disordered classical wave systems for both scalar and vector polarization. In both cases a careful analysis of the long-wavelength limit rediscovered well-known results and, in ad-

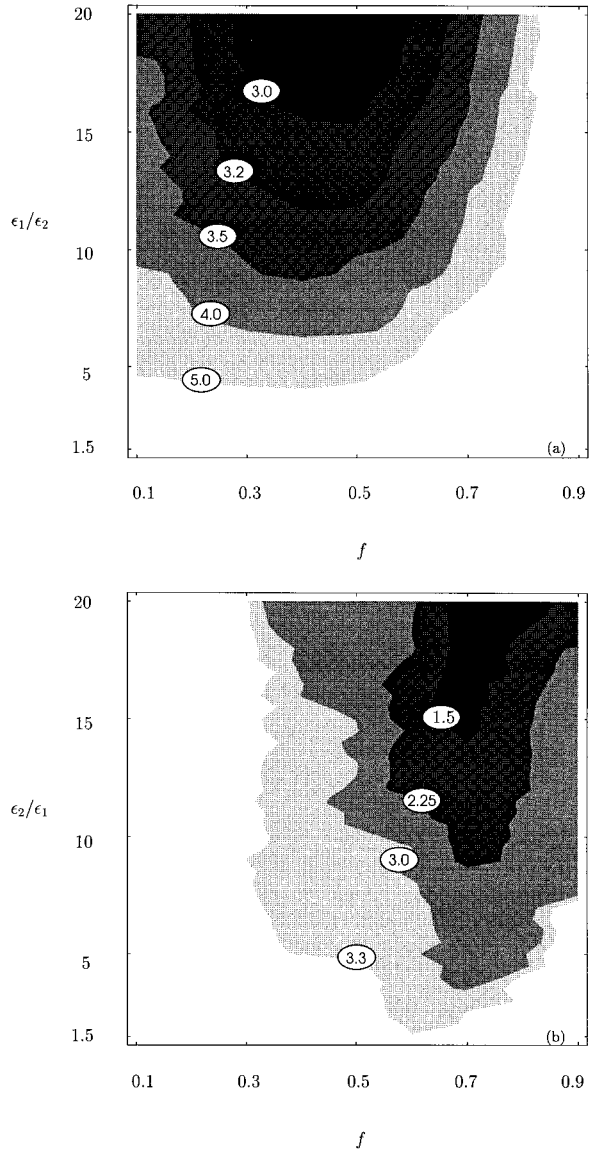

FIG. 6. Contour plot of the localization parameter $\overline{k\ell}_t$ for electromagnetic waves in three dimensions in the direct (a) and the inverse (b) structure for various filling factors f and dielectric contrasts $\epsilon_1 > \epsilon_2$ (a) and $\epsilon_2 > \epsilon_1$ (b).

dition, we have compared them with independent studies on the long-wavelength behavior of two-dimensional photonic crystals. Notably, for the vector polarization pronounced differences appear for different topologies, i.e., for direct and inverse structures, whereas the scalar polarizations are insensitive to topology. For finite frequencies the computational effort as compared to approaches based on an average TCS (Refs. 14 and 15) is drastically reduced and reliable results for transport properties for all values of filling fractions and dielectric contrasts have been obtained. These results are consistent with the results of the theory of van Albada[9] as well as the coated CPA (Ref. 15) in their respective regimes of applicability. Interesting differences in the transport properties between scalar and vector polarization are predicted. Unfortunately, to date there are no experimental data available to judge about these findings. We also have performed a detailed study of the localization parameter in both two- and three-dimensional systems. As a result we were led to conclude that in the direct structure scalar waves are easier to localize than vector waves, whereas the opposite is true in the inverse structure. However, localization is generally favored in the inverse structure, since the localization parameter $\overline{k\ell}_t$ takes on lower values in the inverse structure. Furthermore, we found that for optimal realization of localization there exists a relatively narrow range for the filling factor that depends on the polarization and the structure. These very interesting predictions could be studied experimentally by measuring the localization length near the optimal parameter values in a way similar to existing studies in one-dimensional systems.[32]

ACKNOWLEDGMENTS

We want to thank Peter Wölfle and Johann Kroha for many very helpful discussions. Ames Laboratory is operated for the U.S. Department of Energy by Iowa State University under contract No. W-7405-ENG-82. This work was supported by the Director of Energy Research, Office of Basic Energy Sciences and NATO Grant No. CRG 940647. K.B. acknowledges the support by the Sonderforschungsbereich 195, ''Lokalisierung von Elektronen in makroskopischen und mikroskopischen Systemen'' at the University of Karlsruhe as well as the support by the German Israeli Foundation (GIF).

APPENDIX A: SCATTERING BY A COATED CYLINDER

In this appendix, we define the notations for scattering of plane waves by an infinitely extended coated cylinder. The direction of propagation of the plane wave is assumed to be perpendicular to the cylinders axis. Compared to Ref. 14 we have made the notation more compact and corrected two minor misprints.

The vector cylindrical harmonics for perpendicular incidence are[33]

$$\vec{M}^Z_{nk}(r,\phi) = \left(in \frac{Z_n(kr)}{kr} \hat{r} - Z_n'(kr)\hat{\phi} \right) k e^{in\phi} \qquad \text{(A1)}$$

$$\vec{N}^Z_{nk}(r,\phi) = \frac{1}{k} \nabla \times \vec{M}^Z_{nk}(kr) = Z_n(kr) e^{in\phi} \hat{\phi}, \qquad \text{(A2)}$$

where, in cylindrical coordinates, $\hat{r} = (\cos\phi, \sin\phi, 0)$, $\hat{\phi} = (-\sin\phi, \cos\phi, 0)$, and $\hat{z} = (0,0,1)$. $k = \sqrt{\epsilon}\omega/c$ is the wave number in the homogeneous medium with dielectric constant ϵ, n is the order of the Bessel functions involved, $r = |\vec{r}|$, and the prime denotes the derivative with respect to the argument. Z_n may be any of the following functions: J_n, Y_n (Bessel function of first or second kind of order n), $H_n^{\pm} = J_n \pm i Y_n$ (Hankel function of the first or second kind of order n). We consider a coated cylinder (coating and core dielectric constants ϵ_2 and ϵ_1, respectively) embedded in a homogeneous medium with dielectric constant ϵ_3. Defining for $i = 1,2,3$ the wave numbers $k_i = \sqrt{\epsilon_i}\omega/c$ we may write the expansion of the electric fields inside the core, coating, and surrounding medium as

$$\vec{E}_1(r,\phi)=\frac{1}{k_1}\sum_{n=-\infty}^{\infty}(-i)^n(E_n\vec{M}^J_{nk_1}+F_n\vec{N}^J_{nk_1}) \quad \text{(A3)}$$

$$\vec{E}_2(r,\phi)=\frac{1}{k_2}\sum_{n=-\infty}^{\infty}(-i)^n(G_n\vec{M}^J_{nk_2}+L_n\vec{N}^J_{nk_2}I_n\vec{M}^Y_{nk_2}+K_n\vec{N}^Y_{nk_2}) \quad \text{(A4)}$$

$$\vec{E}_3(r,\phi)=E_{\rm i}(r,\phi)+E_{\rm s}(r,\phi) \quad \text{(A5)}$$

$$\vec{E}_{\rm s}(r,\phi)=\frac{1}{k_3}\sum_{n=-\infty}^{\infty}(-i)^n(C_n\vec{M}^{H^+}_{nk_3}+D_n\vec{N}^{H^+}_{nk_1}). \quad \text{(A6)}$$

The expressions for the magnetic fields can be obtained from Eqs. (A3), (A4), and (A6) by using $\vec{H}=\nabla\times\vec{E}/i\omega\mu_0$ and Eqs. (A1) and (A2). The incident field $\vec{E}_{\rm i}$ for the scalar polarization is

$$\vec{E}^{\parallel}_{\rm i}(r,\phi)=\hat{z}e^{-ikr\cos\phi}, \quad \text{(A7)}$$

whereas for the vector polarization it is given by

$$\vec{E}^{\perp}_{\rm i}(r,\phi)=(\hat{r}\sin\phi+\hat{\phi}\cos\phi)e^{-kr\cos\phi}. \quad \text{(A8)}$$

It is now straightforward to match the boundary conditions at the inner radius R (coating-core) and the outer radius $R_{\rm c}$ (surrounding medium coating) for the two polarizations. However, before we give the results, we find it useful to define a set of abbreviations:

$$P^1_n=\frac{\pi\,{\rm R}}{2}[k_1J'_n(k_1\,{\rm R})J_n(k_2\,{\rm R})-k_2J_n(k_1\,{\rm R})J'_n(k_2\,{\rm R})], \quad \text{(A9)}$$

$$P^2_n=\frac{\pi\,{\rm R}}{2}[k_2J'_n(k_1\,{\rm R})J_n(k_2\,{\rm R})-k_1J_n(k_1\,{\rm R})J'_n(k_2\,{\rm R})], \quad \text{(A10)}$$

$$P^3_n=\frac{\pi\,{\rm R}}{2}[k_2J'_n(k_1\,{\rm R})Y_n(k_2\,{\rm R})-k_1J_n(k_1\,{\rm R})Y'_n(k_2\,{\rm R})], \quad \text{(A11)}$$

$$P^4_n=\frac{\pi\,{\rm R}}{2}[k_1J'_n(k_1\,{\rm R})Y_n(k_2\,{\rm R})-k_2J_n(k_1\,{\rm R})Y'_n(k_2\,{\rm R})], \quad \text{(A12)}$$

$$P^{10}_n=k_3J_n(k_2\,{\rm R_c})H'_n(k_3\,{\rm R_c})-k_2J'_n(k_2\,{\rm R_c})H_n(k_3\,{\rm R_c}), \quad \text{(A13)}$$

$$P^{11}_n=k_2J_n(k_2\,{\rm R_c})H'_n(k_3\,{\rm R_c})-k_3J'_n(k_2\,{\rm R_c})H_n(k_3\,{\rm R_c}), \quad \text{(A14)}$$

$$P^{12}_n=k_2Y_n(k_2\,{\rm R_c})H'_n(k_3\,{\rm R_c})-k_3Y'_n(k_2\,{\rm R_c})H_n(k_3\,{\rm R_c}), \quad \text{(A15)}$$

$$P^{13}_n=k_3Y_n(k_2\,{\rm R_c})H'_n(k_3\,{\rm R_c})-k_2Y'_n(k_2\,{\rm R_c})H_n(k_3\,{\rm R_c}), \quad \text{(A16)}$$

$$P^{14}_n=k_2J'_n(k_2\,{\rm R_c})J_n(k_3\,{\rm R_c})-k_3J_n(k_2\,{\rm R_c})J'_n(k_3\,{\rm R_c}), \quad \text{(A17)}$$

$$P^{15}_n=k_2Y'_n(k_2\,{\rm R_c})J_n(k_3\,{\rm R_c})-k_3Y_n(k_2\,{\rm R_c})J'_n(k_3\,{\rm R_c}), \quad \text{(A18)}$$

$$P^{16}_n=k_3J'_n(k_2\,{\rm R_c})J_n(k_3\,{\rm R_c})-k_2J_n(k_2\,{\rm R_c})J'_n(k_3\,{\rm R_c}), \quad \text{(A19)}$$

$$P^{17}_n=k_2Y'_n(k_2\,{\rm R_c})J_n(k_3\,{\rm R_c})-k_3Y_n(k_2\,{\rm R_c})J'_n(k_3\,{\rm R_c}). \quad \text{(A20)}$$

For the scalar polarization the results for the scattering coefficients then read as

$$C^{\parallel}_n=E^{\parallel}_n=G^{\parallel}_n=I^{\parallel}_n=0, \quad \text{(A21)}$$

$$F^{\parallel}_n=\frac{2i}{\pi\,{\rm R_c}}\frac{1}{P^1_nP^{13}_n-P^4_nP^{10}_n}, \quad \text{(A22)}$$

$$L^{\parallel}_n=-P^4_nF^{\parallel}_n, \quad \text{(A23)}$$

$$K^{\parallel}_n=P^1_nF^{\parallel}_n, \quad \text{(A24)}$$

$$D^{\parallel}_n=\frac{P^1_nP^{13}_n-P^4_nP^{10}_n}{P^1_nP^{15}_n-P^4_nP^{14}_n}, \quad \text{(A25)}$$

whereas we obtain for the vector polarization

$$D^{\perp}_n=F^{\perp}_n=L^{\perp}_n=K^{\perp}_n=0, \quad \text{(A26)}$$

$$E_n^{\perp}=\frac{2}{\pi\,\mathrm{R_c}}\frac{1}{P_n^2P_n^{12}-P_n^3P_n^{11}}, \tag{A27}$$

$$G_n^{\perp}=-P_n^3E_n^{\perp}, \tag{A28}$$

$$I_n^{\perp}=P_n^2E_n^{\perp}, \tag{A29}$$

$$C_n^{\perp}=i\frac{P_n^3P_n^{16}-P_n^2P_n^{17}}{P_n^2P_n^{12}-P_n^3P_n^{11}}. \tag{A30}$$

The problem of obtaining the t matrix for the coated cylinder is thus reduced to a study of the asymptotic behavior of the scattered field, i.e., Eq. (A6). Using the asymptotic expansions of the Hankel functions[33,34] we obtain

$$t_{\vec{k}\vec{k}}(\omega)=-4i\left(a_0^{\parallel/\perp}+2\sum_{l=0}^{\infty}a_l^{\parallel/\perp}\right). \tag{A31}$$

Here $a_l^{\parallel,\perp}$ denote the scattering coefficients for the outside field for the respective polarizations: $a_l^{\parallel}=D_l^{\parallel}$ and $a_l^{\perp}=-iC_l^{\perp}$.

APPENDIX B: ENERGY CONTENT OF A COATED CYLINDER

Using the notations of Appendix A we derive the expressions for the energy content of a coated cylinder illuminated by a plane wave and briefly outline its numerical evaluation (for a similar treatment see Ref. 35)

The energy contents $W^{\parallel}$ and $W^{\perp}$ per unit length for scalar and vector polarization, respectively, may be calculated by integrating Eq. (2) over a disk of radius R_c and using the expressions for the fields, i.e., Eqs. (A3) and (A4). The result may be expressed compactly in terms of

$$\sigma_n^{Z\tilde{Z}}(a,b)=\int_a^b dx x\left[Z_n(x)\tilde{Z}_n(x)\left(1+\frac{n^2}{x^2}\right)+Z_n'(x)\tilde{Z}_n'(x)\right], \tag{B1}$$

where Z and $\tilde{Z}$ stand for any Bessel or Hankel function:

$$\begin{aligned}W^{\parallel}=&\frac{\pi}{2\mu_0\omega^2}\sum_{n=-\infty}^{\infty}|F_n^{\parallel}|^2[\sigma_n^{JJ}(k_1\,\mathrm{R},0)\\&+(P_n^4)^2\sigma_n^{JJ}(k_2\,\mathrm{R_c},k_2\,\mathrm{R})+(P_n^1)^2\sigma_n^{YY}(k_2\,\mathrm{R_c},k_2\,\mathrm{R})\\&-2P_n^1P_n^4\sigma_n^{JY}(k_2\,\mathrm{R_c},k_2\,\mathrm{R})]\end{aligned} \tag{B2}$$

$$\begin{aligned}W^{\perp}=&\frac{\pi}{2\mu_0\omega^2}\sum_{n=-\infty}^{\infty}|E_n^{\perp}|^2[\sigma_n^{JJ}(k_1\,\mathrm{R},0)\\&+(P_n^3)^2\sigma_n^{JJ}(k_2\,\mathrm{R_c},k_2\,\mathrm{R})+(P_n^2)^2\sigma_n^{YY}(k_2\,\mathrm{R_c},k_2\,\mathrm{R})\\&-2P_n^2P_n^3\sigma_n^{JY}(k_2\,\mathrm{R_c},k_2\,\mathrm{R})].\end{aligned} \tag{B3}$$

For numerical purposes it is more efficient to transform Eq. (B1) with the help of the recurrence relations for the Bessel functions into an expression that allows a recursive calculation:[34]

$$\sigma_n^{Z\tilde{Z}}=\kappa_n^{Z\tilde{Z}}+\kappa_{n-1}^{Z\tilde{Z}}-n[Z_n(x)\tilde{Z}_n(x)]_a^b \tag{B4}$$

$$\kappa_n^{Z\tilde{Z}}(a,b)=\int dx x Z_n(x)\tilde{Z}_n(x) \tag{B5}$$

$$\kappa_{n+1}^{Z\tilde{Z}}(a,b)=\kappa_{n-1}^{Z\tilde{Z}}(a,b)-2n[Z_n(x)\tilde{Z}_n(x)]_a^b. \tag{B6}$$

Since the recursion is numerically stable, we only need to compute $\kappa_1^{Z\tilde{Z}}(a,b)$ and $\kappa_0^{Z\tilde{Z}}(a,b)$:[34]

$$\kappa_0^{Z\tilde{Z}}(a,b)=\left[\frac{x^2}{2}[Z_0(x)\tilde{Z}_0(x)+Z_1(x)\tilde{Z}_1(x)]\right]_a^b, \tag{B7}$$

$$\begin{aligned}\kappa_1^{Z\tilde{Z}}(a,b)=&\left[\frac{x^2}{2}[Z_0(x)\tilde{Z}_0(x)+2Z_1(x)\tilde{Z}_1(x)\right.\\&\left.+Z_2(x)\tilde{Z}_2(x)]\right]_a^b-[Z_1(x)\tilde{Z}_1(x)]_a^b.\end{aligned} \tag{B8}$$

APPENDIX C: LONG-WAVELENGTH LIMIT FOR TWO-DIMENSIONAL PHOTONIC CRYSTALS

In this appendix we present the details of obtaining the long-wavelength dielectric constant for two-dimensional photonic crystals. We closely follow the lines of Ref. 27. It is worth mentioning that, although we used this technique for cylindrical scatterers only, it can be applied to any kind of scatterer.

We begin with the scalar polarization in which case the z component of the electric field $E(\vec{r})$ obeys the scalar wave equation

$$\Delta E(\vec{r})+\frac{\omega^2}{c^2}\epsilon_p(\vec{r})E(\vec{r})=0, \tag{C1}$$

where $\Delta=\partial_x^2+\partial_y^2$, $\vec{r}=(x,y)$ and $\epsilon_p(\vec{r})$ is the lattice periodic dielectric function,

$$\epsilon_p(\vec{r})=\epsilon_2+(\epsilon_1-\epsilon_2)\sum_{\vec{R}}S(\vec{r}-\vec{R}). \tag{C2}$$

Here, $\vec{k}=(k_x,k_y)$ and $S(\vec{r})=1$ if $|\vec{r}|<\mathrm{R}$ and zero elsewhere. $\vec{R}=l_1\vec{a}_1+l_2\vec{a}_2$, ($l_1,l_2$ integer), are the lattice vectors spanned by the primitive translations $\vec{a_1}=(a_1^{(1)},a_1^{(2)})$ and $\vec{a_2}=(a_2^{(1)},a_2^{(2)})$. Then, the Fourier expansions of the electric field E and the dielectric constant ϵ_p are of the following form:

$$E(\vec{r})=\sum_{\vec{G}}E_{\vec{G}}e^{i(\vec{k}+\vec{G})\vec{r}} \tag{C3}$$

$$\epsilon_p(\vec{r})=\sum_{\vec{G}}\tilde{\epsilon}_{\vec{G}}e^{i\vec{G}\vec{r}} \tag{C4}$$

$$\tilde{\epsilon}_{\vec{G}}=\frac{1}{\Omega}\int_{\mathrm{WSC}}d^2r\,\epsilon_p(\vec{r})e^{-i\vec{G}\vec{r}}, \tag{C5}$$

where Ω stands for the volume of the Wigner-Seitz cell (WSC). $\vec{G}=h_1\vec{b}_1+h_2\vec{b}_2$, ($h_1,h_2$ integer), are the corresponding two-dimensional reciprocal lattice vectors gener-

ated by the primitive vectors $\vec{b_1}=(2\pi/\Omega)(a_2^{(2)},-a_1^{(2)})$ and $\vec{b_2}=(2\pi/\Omega)(-a_2^{(1)},a_1^{(1)})$. Inserting Eqs. (C3) and (C4) into Eq. (C1) results in

$$E_{\vec{G}}=\frac{\omega^2}{\vec{k}^2c^2}\sum_{\vec{G}'}\frac{\vec{k}^2}{|\vec{k}+\vec{G}|^2}\tilde{\epsilon}_{\vec{G}-\vec{G}'}E_{\vec{G}'} \tag{C6}$$

$$\simeq\frac{\omega^2}{\vec{k}^2c^2}\tilde{\epsilon}_0E_{\vec{G}}. \tag{C7}$$

Here we have used the fact that in the long-wavelength limit $|\vec{k}|\to 0$ only the $\vec{G}=0$ term survives. In this limit, we may define the effective dielectric constant for photonic crystals via $\epsilon_\infty^{-1}=(\omega^2/c^2)/\vec{k}^2$ as $|\vec{k}|\to 0$ and, thus, we obtain the scalar long-wavelength result of Eq. (9), i.e.,

$$\epsilon_\infty^{\parallel}\equiv\tilde{\epsilon}_0\equiv f\epsilon_1+(1-f)\epsilon_2. \tag{C8}$$

A similar procedure may be utilized in the case of vector polarization: The electric field is now perpendicular to the z axis $\vec{E}(\vec{r})=[E_x(\vec{r}),E_y(\vec{r}),0]$ and obeys the vector wave equation

$$-\vec{\nabla}\times\vec{\nabla}\times\vec{E}(\vec{r})+\frac{\omega^2}{c^2}\epsilon_p(\vec{r})\vec{E}(\vec{r})=0. \tag{C9}$$

Since the z component is irrelevant, we may switch to a two-component description of the electric field $\vec{E}(\vec{r})=[E_x(\vec{r}),E_y(\vec{r})]$, where $\vec{r}=(x,y)$. A Fourier expansion analogous to Eq. (C3) and (C4) yields the corresponding wave equation in Fourier space,

$$\mathcal{Q}_{\vec{k}+\vec{G}}\vec{E}_{\vec{G}}=\frac{\omega^2}{c^2}\sum_{\vec{G}'}\tilde{\epsilon}_{\vec{G}-\vec{G}'}\vec{E}_{\vec{G}'}, \tag{C10}$$

where $\vec{k}$ and $\vec{G}$ are, again, two-dimensional vectors. The matrix $\mathcal{Q}_{\vec{k}}$ is given by $\mathcal{Q}_{\vec{k}}=|\vec{k}|^2(\mathcal{E}-\hat{k}\hat{k}^T)$ $\hat{k}=\vec{k}/|\vec{k}|$, where $\hat{k}\hat{k}^T$ is the dyadic formed by $\hat{k}$ and $\mathcal{E}$ is the 2×2 unit matrix. We now introduce a unit vector $\hat{e}_{\vec{G}}$ parallel and another unit vector $\hat{n}_{\vec{G}}$ perpendicular to the vector $\vec{k}+\vec{G}$ and define the components of the electric fields Fourier components along these vectors:

$$\vec{E}_G=E_{\vec{G}}^{\parallel}\hat{e}_{\vec{G}}+E_{\vec{G}}^{\perp}\hat{n}_{\vec{G}}. \tag{C11}$$

Furthermore, we define the matrices ϵ_{LL}, ϵ_{LT}, ϵ_{TL}, and ϵ_{LL} according to

$$\epsilon_{LL}^{\vec{G}\vec{G}'}=\tilde{\epsilon}_{\vec{G}-\vec{G}'}(\hat{e}_{\vec{G}}\cdot\hat{e}_{\vec{G}'}), \tag{C12}$$

$$\epsilon_{LT}^{\vec{G}\vec{G}'}=\tilde{\epsilon}_{\vec{G}-\vec{G}'}(\hat{e}_{\vec{G}}\cdot\hat{n}_{\vec{G}'}), \tag{C13}$$

$$\epsilon_{TL}^{\vec{G}\vec{G}'}=\tilde{\epsilon}_{\vec{G}-\vec{G}'}(\hat{n}_{\vec{G}}\cdot\hat{e}_{\vec{G}'}), \tag{C14}$$

$$\epsilon_{TT}^{\vec{G}\vec{G}'}=\tilde{\epsilon}_{\vec{G}-\vec{G}'}(\hat{n}_{\vec{G}}\cdot\hat{n}_{\vec{G}'}). \tag{C15}$$

Projecting now Eq. (C10) onto $\hat{e}_{\vec{G}}$ and $\hat{n}_{\vec{G}}$, respectively, inserting the first projected equation into the second and taking the $|\vec{k}|\to 0$ limit results in an expression for the long-wavelength effective dielectric constant $\epsilon_\infty^{\perp}$ for the vector polarization,

$$\epsilon_\infty^{\perp}=\epsilon_{TT}^{\vec{G}=0,\vec{G}'=0}-\sum_{\vec{G}''}\sum_{\vec{G}'''}\epsilon_{TL}^{\vec{G}=0,\vec{G}''}(\epsilon_{LL}^{-1})^{\vec{G}'',\vec{G}'''}\epsilon_{LT}^{\vec{G}'''\vec{G}'=0}. \tag{C16}$$

We have evaluated Eq. (C16) numerically as a function of the filling ratio f for the case of square and triangular lattices and dielectric constants $\epsilon_1=9$ and $\epsilon_2=1$ using 717 plane waves to ensure convergence. The results of this evaluation are shown in Fig. 1.

*Present address: Department of Physics, University of Toronto, 60 St. George St., Toronto, Ont., Canada M5S 1A7.

[1] For a review, see *Scattering and Localization of Classical Waves in Random Media*, edited by Ping Sheng (World Scientific, Singapore, 1990).

[2] *Photonic Band Gaps and Localization*, edited by C. M. Soukoulis (Plenum, New York, 1993).

[3] Y. Kuga and A. Ishimaru, J. Opt. Soc. Am. A **1**, 831 (1984); M. P. van Albada and A. Lagendijk, Phys. Rev. Lett. **55**, 2692 (1985); P. E. Wolf and G. Maret, *ibid.* **55**, 2696 (1985); S. Etemad, R. Thompson, and M. J. Andrejco, *ibid.* **57**, 575 (1986); M. Kaveh, M. Rosenbluh, I. Edrei, and I. Freund, *ibid.* **57**, 2049 (1986); F. C. MacKintosh and S. John, Phys. Rev. B **37**, 1884 (1988).

[4] *Photonic Band Gap Materials*, edited by C. M. Soukoulis (Kluwer Academic, Dordrecht, 1996).

[5] Bart A. van Tiggelen, Phys. Rev. Lett. **75**, 422 (1995).

[6] B. A. van Tiggelen, R. Maynard, and A. Heiderich, Phys. Rev. Lett. **77**, 639 (1996); H. Stark and T. C. Lubensky, *ibid.* **77**, 2229 (1996).

[7] P. W. Anderson, Phys. Rev. **109**, 1492 (1958).

[8] P. Sheng and Z. Q. Zhang, Phys. Rev. Lett. **57**, 1879 (1986); C. A. Condat and T. R. Kirkpatrick, *ibid.* **58**, 226 (1987); C. M. Soukoulis, E. N. Economou, G. S. Grest, and M. H. Cohen, *ibid.* **62**, 575 (1989).

[9] M. P. van Albada, B. A. van Tiggelen, A. Lagendijk, and A. Tip, Phys. Rev. Lett. **66**, 3132 (1991); B. A. van Tiggelen, A. Lagendijk, M. P. van Albada, and A. Tip, Phys. Rev. B **45**, 12 233 (1992).

[10] N. Garcia, A. Z. Genack, and A. A. Lisyansky, Phys. Rev. B **46**, 14 475 (1992); A. A. Lisyansky *et al.*, in *Photonic Band Gaps and Localization* (Ref. 2), p. 171.

[11] E. Kogan and M. Kaveh, Phys. Rev. B **46**, 10 636 (1992); G. Cwilich and Y. Fu, *ibid.* **46**, 12 015 (1992); Yu. N. Barabanenkov and V. Ozrin, Phys. Rev. Lett. **69**, 1364 (1992); J. Kroha, C. M. Soukoulis, and P. Wölfle, Phys. Rev. B **47**, 11 093 (1993); B. A. van Tiggelen, A. Lagendijk, and A. Tip, Phys. Rev. Lett. **71**, 1284 (1993); B. A. van Tiggelen and A. Lagendijk, Europhys. Lett. **23**, 311 (1993).

[12] D. Livdan and A. A. Lisyansky, Phys. Rev. B **53**, 14 843 (1996).

[13] Yu. N. Barabanenkov, L. M. Zurk, and M. Yu. Barabanenkov, J. Electromagn. Waves Appl. **9**, 1393 (1995).

[14] C. M. Soukoulis, S. Datta, and E. N. Economou, Phys. Rev. B **49**, 3800 (1994); K. Busch, C. M. Soukoulis, and E. N. Economou, *ibid.* **50**, 93 (1994).

[15] K. Busch, C. M. Soukoulis, and E. N. Economou, Phys. Rev. B **52**, 10 834 (1995).

[16] S. L. McCall *et al.*, Phys. Rev. Lett. **67**, 2017 (1991); W. M. Robertson *et al.*, *ibid.* **68**, 2023 (1992); U. Grüning, V. Lehmann, and C. M. Engelhardt, Appl. Phys. Lett. **66**, 3254 (1995); U. Grüning, V. Lehmann, S. Ottow, and K. Busch, *ibid.* **68**, 747 (1996).
[17] M. M. Sigalas, C. M. Soukoulis, C. T. Chan, and D. Turner, Phys. Rev. B **53**, 8340 (1996).
[18] K. Busch and C. M. Soukoulis, Phys. Rev. Lett. **75**, 3442 (1995).
[19] K. Busch and C. M. Soukoulis, Phys. Rev. B **54**, 893 (1996).
[20] A. Gonis, *Green Functions for Ordered and Disordered Systems* (North-Holland, Elsevier, New York, 1992).
[21] X. Jing, P. Sheng, and M. Zhou, Phys. Rev. A **46**, 6513 (1992); Physica A **207**, 37 (1994).
[22] Ping Sheng, *Introduction to Wave Scattering, Localization and Mesoscopic Phenomena* (Academic, New York, 1995).
[23] M. Kafesaki and E. N. Economou, Europhys. Lett. **37**, 7 (1997).
[24] D. A. G. Brüggeman, Ann. Phys. (Leipzig) **24**, 636 (1935).
[25] J. C. Maxwell-Garnett, Philos. Trans. R. Soc. London **A203**, 385 (1904).
[26] D. J. Bergman, Ann. Phys. (N.Y.) **138**, 78 (1982).
[27] S. Datta, C. T. Chan, K. M. Ho, and C. M. Soukoulis, Phys. Rev. B **48**, 14 936 (1993).
[28] G. W. Milton, R. C. McPhedran, and D. R. McKenzie, Appl. Phys. **25**, 23 (1981).
[29] J. H. Page, H. P. Schriemer, A. E. Bailey, and D. A. Weitz, Phys. Rev. E **52**, 3106 (1995); J. H. Page *et al.*, Science **271**, 634 (1996).
[30] E. N. Economou, C. M. Soukoulis, and A. D. Zdetsis, Phys. Rev. B **30**, 1686 (1984); A. D. Zdetsis, C. M. Soukoulis, E. N. Economou, and G. Grest, *ibid.* **32**, 7811 (1985).
[31] E. Abrahams, P. W. Anderson, D. C. Licciardello, and T. V. Ramakrishnan, Phys. Rev. Lett. **42**, 673 (1979).
[32] Z. Daozhang *et al.*, Phys. Rev. B **50**, 9810 (1994); Z. Q. Zhang *et al.*, *ibid.* **54**, 11 891 (1996).
[33] C. F. Bohren and D. R. Huffman, *Absorption and Scattering of Light by Small Particles* (Wiley Interscience, New York, 1983).
[34] G. N. Watson, *A Treatise on the Theory of Bessel Functions*, 2nd ed. (Cambridge Univeristy Press, Cambridge, 1952).
[35] A. Bott and W. Zdunkowski, J. Opt. Soc. Am. A **4**, 1361 (1987).